

Electrophoretic deposition of mesoporous bioactive glass on glass-ceramic foam scaffolds for bone tissue engineering

*Original*

Electrophoretic deposition of mesoporous bioactive glass on glass-ceramic foam scaffolds for bone tissue engineering / Fiorilli, SONIA LUCIA; BAINO, Francesco; CAUDA, VALENTINA ALICE; CREPALDI, M.; VITALE BROVARONE, Chiara; DEMARCHI, Danilo; ONIDA, Barbara. - In: JOURNAL OF MATERIALS SCIENCE. MATERIALS IN MEDICINE. - ISSN 1573-4838. - ELETTRONICO. - 26:1(2015), pp. 1-12. [10.1007/s10856-014-5346-6]

*Availability:*

This version is available at: 11583/2586162 since: 2021-04-08T12:57:37Z

*Publisher:*

Springer

*Published*

DOI:10.1007/s10856-014-5346-6

*Terms of use:*

This article is made available under terms and conditions as specified in the corresponding bibliographic description in the repository

*Publisher copyright*

Springer postprint/Author's Accepted Manuscript

This version of the article has been accepted for publication, after peer review (when applicable) and is subject to Springer Nature's AM terms of use, but is not the Version of Record and does not reflect post-acceptance improvements, or any corrections. The Version of Record is available online at: <http://dx.doi.org/10.1007/s10856-014-5346-6>

(Article begins on next page)

# **Electrophoretic deposition of mesoporous bioactive glass on glass-ceramic foam scaffolds for bone tissue engineering**

Sonia Fiorilli<sup>a</sup>, Francesco Baino<sup>a</sup>, Valentina Cauda<sup>b</sup>, Marco Crepaldi<sup>b</sup>, Chiara Vitale Brovarone<sup>a,c</sup>, Danilo Demarchi<sup>d</sup>, Barbara Onida<sup>a\*</sup>

<sup>a</sup> Dipartimento di Scienza Applicata e Tecnologia, Politecnico di Torino, Corso Duca degli Abruzzi 24, 10129 Torino, Italy

<sup>b</sup> Center for Space Human Robotics@PoliTo, Istituto Italiano di Tecnologia, Corso Trento 21 10129 Torino, Italy

<sup>c</sup> Bionica Tech S.r.l, Corso Sommelier 32, 10128 Torino, Italy

<sup>d</sup> Dipartimento di Elettronica e Telecomunicazioni Politecnico di Torino, Corso Duca degli Abruzzi 24, 10129 Torino, Italy

\*Corresponding author: Tel: +39 011 0904631; E-mail: barbara.onida@polito.it

## **Abstract**

In this work, the coating of 3-D foam-like glass-ceramic scaffolds with a bioactive mesoporous glass (MBG) was investigated. The starting scaffolds, based on a non-commercial silicate glass (SCNA), were fabricated by the polymer sponge replica technique followed by sintering; then, electrophoretic deposition (EPD) was applied to deposit a MBG layer on the scaffold struts. EPD was also compared with other techniques (dipping and direct *in situ* gelation) and it was shown to lead to the most promising results. The scaffold pore structure was maintained after the MBG coating by EPD, as assessed by SEM and micro-CT. *In vitro* bioactivity of the scaffolds was assessed by immersion in simulated body fluid (SBF) and subsequent evaluation of hydroxyapatite (HA) formation. The deposition of a MBG coating can be a smart strategy to impart bioactive properties to the scaffold, allowing the formation of nano-structured HA agglomerates within 48 h

from immersion, which does not occur on uncoated scaffold surfaces. The mechanical properties of the scaffold do not vary after the EPD (compressive strength  $\sim 19$  MPa, fracture energy  $\sim 1.2 \times 10^6$  J  $\text{m}^{-3}$ ) and suggest the suitability of the prepared highly bioactive constructs as bone tissue engineering implants for load-bearing applications.

**Keywords:** Electrophoresis; Scaffold; Mesoporous glass; Bioactivity; Bone tissue engineering.

## 1. Introduction

Since the invention of 45S5 Bioglass<sup>®</sup> by Hench and co-workers in 1969 [1], bioactive glasses and glass-ceramics have been widely investigated as ideal materials for bone tissue engineering applications due to their ability to form an interfacial bond with host tissues [2] and to stimulate via ion release the genes of cells towards a path of regeneration and self-repair [3]. Over the last three decades, 45S5 Bioglass<sup>®</sup> has been marketed worldwide for clinical use in the form of cast structures to replace the middle ear bones, fine particulate to fill periodontal defects, porous granules and mouldable or injectable paste for orthopaedic applications [4]. 45S5 Bioglass<sup>®</sup> was also experimented to produce 3-D porous scaffolds able to allow tissue in-growth in their porous network. In this regard, the first study was reported in 2001 by Yuan et al. [5], who implanted porous Bioglass<sup>®</sup>-derived glass-ceramic cylinders in dogs; only a small amount of new bone was detected within the implants (around 3% of the pores area on optical cross-sections) as the porosity obtained by H<sub>2</sub>O<sub>2</sub> foaming was low ( $\sim 32$  vol.%) and poorly interconnected. Chen et al. [6] and Vitale-Brovarone et al. [7] pioneered the use of the sponge replication method to fabricate highly porous (85-90 vol.%) Bioglass<sup>®</sup> scaffolds able to allow tissue and blood vessels in-growth; however, these scaffolds were too brittle (compressive strength within 0.3-0.4 MPa [6], 1 MPa [7]) to deem any real surgical application. The combination of PE particles and a polymeric sponge as pore formers [8] as well as various optimization strategies [9] were also reported in the attempt at

improving the mechanical performance of Bioglass<sup>®</sup> scaffolds, but problems of brittleness still remained. This was one of the major reasons why other bioactive glass formulations were developed in recent years in the hope that a truly strong, bioactive glass scaffold can be eventually produced. As emphasized in some recent studies [10-12], the design of an appropriate bioactive glass composition for scaffolding is a complex task to achieve, being a combination of different competing issues. Indeed, a scaffold must guarantee an appropriate surface reactivity and accordingly a good bioactivity, as well as a favourable sinterability versus sufficient crystallization, which is a key parameter to consider for obtaining well-densified, strong struts of the scaffold; in addition an intrinsic mechanical strength of the material is required.

In some recent studies, the authors developed a biocompatible silicate glass (SCNA) in the SiO<sub>2</sub>-CaO-Na<sub>2</sub>O-Al<sub>2</sub>O<sub>3</sub> system and reported various evidences supporting its mechanical suitability for bone repair applications even in load-bearing conditions [13-15]; on the other hand, however, SCNA is characterized by low bioactive properties. In this work, a novel approach to produce a high-strength and bioactive scaffold for bone replacement is disclosed: SCNA scaffold is designed to act as a macroporous substrate on which a highly bioactive coating of mesoporous glass is deposited through electrophoresis. This approach is useful to overcome the limitation of dramatic brittleness of foam-like scaffolds fully constituted of mesoporous bioactive glass (MBG) (compressive strength around 0.05-0.15 MPa [16,17]), which is unavoidably due to the presence of a high, intrinsic mesoporosity of the material. Electrophoretic deposition (EPD) is a special colloidal processing technique that uses the electrophoresis mechanism for the movement of charged particles suspended in a solution under an electric field, with the aim of depositing them on a substrate to develop coatings of adjustable thickness [18]. EPD is characterized by high versatility in terms of the broad range of materials (in particulate form) to which it can be applied and the relatively simple, inexpensive equipment required. The application of EPD in the biomaterials field started with the development of hydroxyapatite (HA) coatings on titanium substrates in the 1980s [19], gaining further impetus one decade later with the work of Zhitomirsky and Gal-Or [20], which

was fundamental for the EPD of HA nanoparticles. Krause et al. [21] were the first to have investigated the EPD of 45S5 Bioglass<sup>®</sup> powder (particle size below 3  $\mu\text{m}$ ) from aqueous suspensions. Roether et al. [22] applied EPD to coat 3-D porous poly(lactic acid) substrates with 45S5 Bioglass<sup>®</sup> particles and Boccacini et al. [23] showed that polyetheretherketone (PEEK)/Bioglass<sup>®</sup> composite coatings can be produced via EPD on nickel-titanium shape memory alloy wires. In the last few years there has been a considerable increase in research efforts to apply EPD to produce polymer/nano-sized bioactive glass composite coatings with enhanced multifunctional properties (e.g. bone-bonding ability and drug release *in situ* via polymer degradation) [24]. The use of EPD to produce carbon nanotubes (CNTs) coatings has been also investigated: for example, Meng et al. [25] incorporated CNTs into Bioglass<sup>®</sup> macroporous foams by EPD and cultured mesenchymal stem cells on the constructs with and without electrical stimulation, and they observed that the electrical conductivity associated to the CNTs can promote the proliferation and differentiation of the cells attached onto the scaffold. Therefore, the applications of EPD in the biomedical sector are being expanded to include a variety of functional, nanostructured and composite coatings with the aim to impart smart added values to biomaterials. To the best of the authors' knowledge, to date the EPD of MBGs has been never reported; thus, this work represents a pilot study that could provide a significant incentive to the development of a new procedure to prepare bioactive scaffolds for bone tissue engineering.

## **2. Materials and methods**

### **2.1. Macroporous scaffolds fabrication**

Bone-like macroporous scaffolds were produced using a quaternary silicate glass (SCNA; 57SiO<sub>2</sub>-34CaO-6Na<sub>2</sub>O-3Al<sub>2</sub>O<sub>3</sub> mol.%) as a starting material. SCNA reagents (high-purity powders of SiO<sub>2</sub>, CaCO<sub>3</sub>, Na<sub>2</sub>CO<sub>3</sub> and Al<sub>2</sub>O<sub>3</sub> purchased from Sigma-Aldrich) were molten in a platinum crucible at

1550 °C for 1 h in air; the melt was quenched in cold water to obtain a frit, that was subsequently ground by using a 6-balls zirconia milling jar and manually sieved (Giuliani stainless steel sieve) to obtain particles with size below 32 µm. The sponge replication method was adopted for fabricating the scaffolds due to its excellent suitability to obtain porous ceramics with a highly-interconnected 3-D network of open macropores [26]. Small cubic blocks (10.0 mm × 10.0 mm × 10.0 mm) of a commercial open-cells polyurethane (PU) sponge (density of the porous polymer ~20 kg m<sup>-3</sup>) were coated with SCNA powder by impregnation in a water-based glass slurry (glass : distilled water : poly(vinyl alcohol) (PVA) = 30 : 64 : 6 wt.%). After PVA hydrolysis under continuous magnetic stirring at 80 °C, SCNA powder was added to the solution; the water evaporated during PVA dissolution was re-added to the slurry to restore the correct weight ratios among the components. After further stirring for 15 min at room temperature to ensure slurry homogeneity, the sponge blocks were immersed for 60 s in the slurry. The slurry infiltrated the porous network of the PU template that was extracted from the slurry and subsequently compressed (50 kPa for 1 s) up to 60% in thickness along three orthogonal spatial directions, in order to homogeneously remove the excess slurry. This infiltration/compression cycle was repeated for three times; then, a final cycle of impregnation without subsequent compression was performed. The samples were dried at room temperature overnight and afterwards thermally treated at 1000 °C for 3 h (heating and cooling rates set at 5 and 10 °C min<sup>-1</sup>, respectively) in order to burn-off the polymeric template and to sinter the inorganic particles. As reported elsewhere [27], one crystalline phase (wollastonite, CaSiO<sub>3</sub>) forms during the above-mentioned heat treatment; however, for the sake of simplicity, the expression “SCNA scaffold” will be hereafter adopted, without further specifying the glass-ceramic nature of the sintered material. SCNA scaffolds were eventually coated by MBG following three different procedures, as described in the section 2.3.

## 2.2. MBG synthesis procedure

The mesostructured glass to be deposited on the macroporous SCNA scaffolds was produced by coupling a traditional sol-gel method with the evaporation-induced self-assembly (EISA) process, following a synthesis procedure reported elsewhere [28] wherein an amphiphilic triblock copolymer with sequence poly(ethylene glycole)-poly(propylene glycole)-poly(ethylene glycole) (PEG-PPG-PEG), commercially called Pluronic 123 (P123), was used as a structure directing agent. Briefly, 2.0 g of P123 ( $M_w = 5800$  Da; Aldrich) were dissolved in 60.0 g of ethanol (99.5%, Sigma-Aldrich) and 1.0 g of 0.5 M HCl. After continuous magnetic stirring (300 rpm) at 35 °C for 1 h till P123 is completely dissolved, the glass oxides precursors, i.e. 6.7 g of tetraethyl orthosilicate (TEOS; 98.0%, Sigma-Aldrich), 0.73 g of triethyl phosphate (TEP; 99.8%, Sigma-Aldrich) and 1.4 g of calcium nitrate tetrahydrate ( $\text{Ca}(\text{NO}_3)_2 \cdot 4\text{H}_2\text{O}$ ; Sigma-Aldrich) (molar ratio  $\text{SiO}_2 : \text{CaO} : \text{P}_2\text{O}_5 = 80 : 15 : 5$ ), were added to the synthesis batch ( $\text{pH} < 1.0$ ). The batch was continuously stirred at 35 °C for 24 h; then, the sol was cast into Petri dishes to undergo the EISA process at room temperature. The gelation occurred by ~36 h; after 7 days of ageing, the dried gels were carefully removed from the moulds as transparent membranes and finally calcined at 700 °C in air for 5 h (heating and cooling rates set at 1 and 10 °C  $\text{min}^{-1}$ , respectively). The glass membranes were then ground and sieved below 20  $\mu\text{m}$  to obtain a suitable powder for EPD, for which the use of particles with size below 30  $\mu\text{m}$  is recommended [29].

## 2.3. MBG coating deposition

### 2.3.1. Electrophoretic deposition (EPD)

The suspension for EPD was prepared by adding to acetone the sieved MBG powder at a concentration of 3 g  $\text{L}^{-1}$ . The resulting suspension was sonicated in an ultrasonic bath for 10 min to

favour the powder dispersion. The EPD was performed using an experimental set-up similar to that reported by Boccacini et al. [30], where the two electrodes are placed in the suspension with the scaffold suspended, through a clamp, in the centre of the EPD cell. The scaffold was placed in such a way that the larger pores were oriented perpendicularly to the surface of the electrodes, and thus to the particles flow. The electrodes, made of platinum foils with dimensions of 15 mm × 15 mm × 0.2 mm, were connected to a dc power supply. EPD was carried out by setting a constant voltage of 200 V, with deposition time of 5 min and electrode separation of 40 mm. After the EPD process, the scaffold was carefully and slowly withdrawn from the EPD cell, dried at room temperature overnight, and then thermally treated at 500 °C (heating rate: 10 °C min<sup>-1</sup>) for 5 h to favour the anchoring of incorporated MBG particles to the scaffold walls.

### 2.3.2. Comparative methods: dipping and direct *in situ* gelation

In addition to the EPD, two other approaches were experimented to coat SCNA macroporous scaffolds with MBG; it is worth anticipating here that both these alternative strategies resulted unsuccessful, but the relevant results are reported in this work to further emphasize the potential of EPD for the intended application.

The first approach consisted of dipping the scaffold for 10 min in a suspension of MBG in acetone at the same concentration used for the EPD, but without applying a voltage, to elucidate the role of the latter in determining the coating features. The scaffold was thermally treated in the same way as reported in the section 2.3.1.

The second approach consisted of driving the MBG incorporation inside the porous scaffold by casting the sol into a Petri dish containing the scaffold till it was completely submerged. In this way, gelation is expected to occur inside scaffold macropores filled with the sol; after 48 h, the scaffold was extracted from the surrounding gel (the soft membrane was manually cut with a



lancet), underwent an ageing phase of 7 days and was finally calcined as reported for the MBG as such (see the section 2.2)

## 2.4. Characterization

### 2.4.1. Morphological and structural characterization

The scaffolds were metal-coated (chromium or silver), and their morphology and porous 3-D architecture were investigated by scanning electron microscopy (JEOL-JX-A8600). The inner porous network of the constructs produced by EPD was also non-destructively investigated by micro-computed tomography (micro-CT; SkyScan 1174, Micro Photonics Inc.; maximum resolution: 6.5  $\mu\text{m}$ ) to assess the pores content and interconnectivity (CTAn software). 3-D reconstruction and visualization were performed using NRecon and DataViewer/CTVox softwares, respectively. For the purpose of comparison, the total porosity of the scaffolds was also calculated through mass-volume measurements as  $(1 - \rho_s / \rho_0) \times 100$ , wherein  $\rho_s$  is the scaffold density (mass/volume ratio) and  $\rho_0$  is the density of bulk material.

The MBG was investigated by means of wide-angle ( $2\theta$  within  $10-70^\circ$ ) and low-angle ( $2\theta$  within  $0.8-4^\circ$ ) X-ray diffraction (XRD, X'Pert Philips diffractometer with Bragg-Brentano camera, Cu anode, and  $K\alpha$  radiation). The X-ray pattern (data not reported) shows an evident peak around  $2\theta = 1.5^\circ$ , which leads to a  $d$ -spacing equal to 5.8 nm, and a broad halo within the range  $2\theta = 20-30^\circ$ , typical of silicate glasses. Nitrogen adsorption-desorption measurement at 77 K (Quantachrome Autosorb1) performed on the MBG ground in powder revealed a typical IV type isotherm (supporting information S1). The specific surface area (SSA), assessed by using the Brunauer-Emmet-Teller (BET) method, resulted 307  $\text{m}^2/\text{g}$ , whereas the pores diameter determined through the DFT (Density Functional Theory) method, using the NLDFT equilibrium model [31], was 4.7 nm.

Compositional investigations were performed by energy dispersive spectroscopy (EDS; Philips Edax 9100).

#### 2.4.2. *In vitro* bioactivity

In the context of silicate glasses for bone regeneration (like those investigated in the present study), the expression “inorganic bioactivity” or simply “bioactivity” refers to the formation of a HA or HA-like layer on the surface of the material after contact with biological fluids. The scaffold bioactive properties were assessed by soaking the samples in an acellular simulated body fluid (SBF) prepared according to the Kokubo’s protocol [32], which is currently considered as a reliable standard medium for assessment of biomaterials behaviour *in vitro*.

MBG-coated and as-such SCNA scaffolds were soaked in 30 ml of SBF contained in PE bottles and maintained at 37 °C in an incubator for 24 h and 48 h, in order to investigate the modifications of the material surface in the short term. At the end of the experiment, the samples were gently washed with distilled water, dried at room temperature, chromium-coated and investigated by SEM and EDS.

#### 2.4.3. Mechanical testing

The compressive failure stress  $\sigma_c$  (MPa) was evaluated through crushing tests (Syntech 9/D testing machine, 44-kN load cell, cross-head speed set at 1 mm min<sup>-1</sup>) as:

$$\sigma_c = \frac{L_M}{A_R} \quad (1)$$

wherein  $L_M$  (N) is the maximum load registered during the test and  $A_R$  (mm<sup>2</sup>) is the resistant cross-sectional area.

The energy per unit volume  $E_v$  ( $\text{J m}^{-3}$ ) absorbed by the scaffold till the breaking off is reached was defined as the energy necessary to deform a specimen from the unloaded condition to the failure strain  $\varepsilon_f$ , and was calculated as the area under the stress-strain curve up to  $\varepsilon_f$  [33]:

$$E_v = \int_0^{\varepsilon_f} \sigma(\varepsilon) d\varepsilon \quad (2)$$

wherein the strain  $\varepsilon$  denotes the integration variable; the initial and final conditions are, respectively,  $\sigma(\varepsilon = 0) = 0$  and  $\sigma(\varepsilon = \varepsilon_f) = \sigma_c$  (calculated from Eq.(1)).

The above-mentioned mechanical parameters were expressed as mean value  $\pm$  standard deviation calculated on seven samples ( $\approx 7 \text{ mm} \times 7 \text{ mm} \times 5 \text{ mm}$  cuboids) for each type.

### 3. Results and discussion

#### 3.1. Morphology

Figure 1a reports a SEM micrograph of a thermally-treated SCNA scaffold, which is a successful replica of the porous polymeric template. The strut architecture, with open and interconnected macropores having size above  $100 \mu\text{m}$ , closely mimics the 3-D trabecular structure of human cancellous bone [34]. The glass-ceramic nature of sintered SCNA is confirmed by Fig. 1b, showing the micro-rough appearance of a scaffold trabecula due to the presence of needle-like crystals developed during the thermal treatment. According to previous works, this crystalline phase can be identified as  $\text{CaSiO}_3$  (wollastonite), as confirmed by the compositional analysis (Fig. 1c).

Figures 2a and 2b show SCNA scaffold after the EPD and thermal treatment at lower and higher magnification, respectively. At the micro-scale, scaffold pore walls and struts appear covered by a rather dense and uniform layer of MBG micro-sized particles, without large agglomeration occluding the macroporous structure. The corresponding EDS spectrum is reported in Fig. 2c: besides the peaks of silicon (Si) and calcium (Ca), also detected for the scaffold as such, the signal

due to phosphorus (P) is observed, as expected on the basis of the MBG composition. Detection of a signal due to phosphorus (P) is a clear evidence of the incorporation of MBG particles inside the SCNA scaffold, as the composition of the latter ( $57\text{SiO}_2\text{-}34\text{CaO-}6\text{Na}_2\text{O-}3\text{Al}_2\text{O}_3$  mol.%) does not imply the presence of P.

For the purpose of comparison, the results of the other two (unsuccessful) strategies experimented in the attempt to incorporate MBG inside the scaffold are illustrated in Figures 3 and 4. Figure 3 shows SCNA scaffold after dipping in MBG suspension: the macropores surface appears mostly uncovered and quite large aggregates (about 20-30  $\mu\text{m}$ ) of MBG particles are observed in few cavities. It appears that, through dipping approach, very low amount of MBG can be loaded inside SCNA macropores and that the few incorporated particles tend to assemble into cavities and coalesce during thermal treatment. EDS analysis performed on these aggregates (Figure 3c) shows, as in the case of MBG incorporated by EPD, the presence of the phosphorus (P) signal.

On the other hand, the strategy of submerging the scaffold within the sol led to an excessive incorporation of MBG, as shown in Fig. 4. Before calcination, the outer surface of the scaffold was coated by a thick layer that apparently obstructed the pores, which made undetectable the macroporous network lying underneath. After the thermal treatment, the problem persisted since a thick, fragmented coating of MBG enveloped the SCNA scaffold and occluded the macropores. Such a situation precludes any biomedical suitability of the device, as the scaffold macropores would not be accessible by biological fluids.

Micro-CT investigations, carried out on the samples processed by EPD, revealed that there was no difference between SCNA scaffold as such and MBG-coated SCNA scaffold in terms of total porosity (total pore contents of 50.9 and 51.6 vol.% were determined, respectively). These findings are consistent with SEM observations, which showed the presence of a thin MBG coating on scaffold struts without pore occlusion. Density measurements substantially confirmed the assessments by micro-CT (mean total porosities of 53.3 and 53.8 vol.% were found for the scaffold as such and the MBG-coated scaffold, respectively). Therefore, the deposition of a MBG thin

coating on scaffold struts via EPD does not involve decrement in the scaffold porosity, that remains unaltered with respect to non-coated samples.

The total porosity of the prepared constructs is within the range recommended for bone tissue engineering scaffolds (50-80 vol.% [35]), although very close to the lower threshold. The scaffolds had good 3-D pores interconnectivity throughout the whole volume with open porosity calculated by CTAn software above 95% of the overall pores content, which is a key feature after *in vivo* implantation in order to have paths for cells to migrate, tissue to grow in and waste products to flow out.

Micro-CT was also used to assess in a non-destructive way whether the coating was homogeneously and continuously deposited on the struts throughout the scaffold volume. The instrument available for the analysis exploited a polychromatic X-ray radiation and, therefore, the discrimination between materials with similar density (SCNA and MBG) was quite difficult; however, after careful post-processing of the reconstructed images, valuable results have been obtained. Figure 5 reports the density mapping along different cross-sections of a MBG-coated SCNA scaffold depending on the different X-ray absorption of the involved materials. The presence of MBG (green colour) is clearly visible in the outer regions of the scaffold volume (periphery), including both the zones underneath the scaffold surfaces perpendicular to the EPD flow and the top and bottom faces of the scaffold (planes parallel to the EPD flow). In the micro-CT reconstructions, the scaffold core is mainly characterized by the colour blue, which indicates the presence of SCNA as the predominant material. Therefore, we can propose that, moving from the outer surfaces to the core, the MBG coating deposited on scaffold struts becomes progressively thinner; it is not possible to exclude its presence in the inner region as it could be thinner than 6.5  $\mu\text{m}$ , which is the best resolution achievable with the used micro-CT equipment, or too discontinuous to be detectable.

### 3.2. Bioactive properties

The need for a bioactive coating to be deposited on SCNA scaffold struts is due to the very poor ability of this material to induce the formation of HA on its surface upon immersion in biological fluids. As shown in Figure 6, even after a long-term soaking in SBF (1 month) the formation of a HA layer did not occur and only the presence of sparse calcium phosphate ultrafine particles can be detected. As reported in literature [1], the bioactive process is a sequence of ion-exchange phenomena occurring between the scaffold material and biological fluids; in the present case, the partial substitution of  $\text{Si}^{4+}$  with  $\text{Al}^{3+}$  ions in the  $\text{Al}_2\text{O}_3$ -rich residual glass phase of sintered glass-ceramic SCNA (the crystalline phase is wollastonite,  $\text{CaSiO}_3$ ) led to a chemically stable network that is barely prone to react with the surrounding fluids. Upon soaking, a thin layer of silica gel formed on scaffold struts, through which it was possible to detect the shape of the wollastonite crystals lying underneath (Figure 6b). These results are consistent with the observations reported by Kokubo et al. [36] for  $\text{Al}_2\text{O}_3$ - and wollastonite-containing biomedical glass-ceramics.

Figure 7a reports a SEM micrograph of MBG-coated SCNA scaffold surface after soaking for 48 h in SBF: it shows a thin layer of silica gel (as in the case of SCNA scaffold as such, see Figure 6) on which newly-formed agglomerates (size within 1-2  $\mu\text{m}$ ) characterized by a “cauliflower” morphology are well distinguishable. Figure 7b shows that these globular agglomerates are constituted by needle-like nano-crystals, and the corresponding EDS analysis on these precipitates (Figure 7c) reveals the presence of calcium and phosphorus with atomic ratio of 1.60 (the high peak of Si visible in the spectrum is due to boundary effects associated to the presence of the thin silica gel layer and SCNA substrate lying underneath). According to the literature, this newly formed phase can be identified as HA: in fact, it is widely reported that precipitates of Ca-deficient HA (Ca/P atomic ratio lower than 1.67, which is the value for stoichiometric HA) with cauliflower morphology typically form on the surface of bioactive glasses upon soaking in SBF [10, 12], as actually observed in the present work (Figure 7). It is worth noting that the nano-crystalline nature of the HA formed on MBG-coated SCNA scaffolds closely mimics the features of the biological apatite of bones [37], whereas synthetic HA commonly used in orthopaedics is characterized by

larger grain size [38]. This fact could have a significant impact on the *in vivo* performance of the scaffold once implanted, as it is known that surface nano-topography is a key factor in determining and mediating cell-substrate interactions [38].

It is worth underlining that the MBG system, despite its large silica content (80 mol. %), is highly bioactive. Hench et al. [39] observed that, for conventional melt-derived glasses, the silica content has to be 60 mol. % or less to allow the bonding with bone. Nevertheless, it was demonstrated that bone bonding can be attained with sol-gel glasses with up to 90 mol. % of SiO<sub>2</sub> because of their high surface area (approximately two orders of magnitude higher than that of melt-derived glasses), which allows the surface reactivity to be emphasized [40, 41]. The remarkable bioactive properties shown by MBG-coated SCNA scaffold are also comparable with those previously reported [28] for MBG membranes (with the same composition) upon soaking in SBF: also in that case, fast formation of HA-like globular agglomerates was observed after 48 h. This suggests that the open mesoporous structure is retained by the bioactive glass when deposited in form of coating by EPD, playing a key role in determining the performances of MBG-coated scaffold in SBF. This is also supported by the evidence that the bioactive kinetics observed for a non-porous bioactive glass coating (45S5 Bioglass<sup>®</sup>) deposited by EPD [42] on stainless steel substrates, resulted slower compared to those reported in the present work: in fact, the initial formation of sparse calcium phosphate deposits (HA precursors) was reported to occur after soaking for 5 days in SBF. In the present study, the electrodeposited MBG coating undergoes partial dissolution upon soaking in SBF due to its high reactivity, thereby accelerating the complex sequence of ion-exchange phenomena which lead to the final formation of HA agglomerates on the biomaterial surface (Fig. 7), as described in detail by Hench et al. [2].

Future studies on the MBG-coated SCNA scaffolds will include *in vitro* tests with cells; however, the biological compatibility of the constituent materials, i.e. MBG powders and SCNA, has been already demonstrated separately in previous studies [28,43], thereby suggesting the biological suitability of the composite system obtained through their combination.

### 3.3. Mechanical properties

The data reported in Table 1 show that, from a mechanical viewpoint, there is no significant difference between the SCNA scaffold as such and the samples coated with MBG, which suggests that EPD does not damage the scaffold structure and integrity. The scaffolds compressive strength is above the standard reference range (2-12 MPa [39]) considered for human trabecular bone as well as most of foam-like scaffolds with the same porosity reported in the literature [11]; therefore, the produced samples can be proposed even for load-bearing applications like in joint prostheses [13,14]. The fracture energy is from one to two orders of magnitude higher than that reported for other glass-ceramic scaffolds produced by the same method and having analogous macroporous architecture [44,45]; in this regard, a key role is played by the formulation of the starting glass (SCNA) in affecting the sintering behaviour of glass particles and the densification of the scaffold struts.

## 4. Conclusions

Glass–ceramic scaffolds, belonging to the  $\text{SiO}_2\text{--CaO--Na}_2\text{O--Al}_2\text{O}_3$  (SCNA) system, have been successfully coated with mesoporous bioactive glass (MBG) by the electrophoretic deposition technique. The MBG layer appears rather dense and uniformly distributed throughout the scaffold walls and struts, without occluding the macroporous structure, as assessed by SEM and micro-CT analyses. Alternative approaches to incorporate MBG, such as dipping and *in situ* gelation, resulted unsuccessful. The bioactivity of the MBG-coated SCNA has been assessed by the formation of globular agglomerates of HA nano-crystals after soaking for just 48 h in SBF, which were not observed on SCNA scaffolds as such even after soaking for longer periods. The mechanical



properties of the MBG coated-SCNA scaffold suggest their suitability as load-bearing high-strength grafts for bone defect restoration; furthermore, thanks to the combination of adequate porosity, high mechanical strength and good bioactivity, their use as smart components of joint prostheses could be envisaged.

## References

- [1] Hench LL. The story of Bioglass<sup>®</sup>. *J Mater Sci: Mater Med*. 2006;17:967-78.
- [2] Hench LL, Splinter RJ, Allen WC, Greenlee TK. Bonding mechanisms at the interface of ceramic prosthetic materials. *J Biomed Mater Res*. 1971;5:117-41.
- [3] Hoppe A, Guldal, Boccaccini AR. A review of the biological response to ionic dissolution products from bioactive glasses and glass-ceramics. *Biomaterials*. 2011;32:2757-54.
- [4] Hench LL. Glass and glass-ceramic technologies to transform the world. *Int J Appl Glass Sci*. 2011;2:162-76.
- [5] Yuan H, De Bruijn JD, Zhang X, Van Blitterswijk CA, De Groot K. Bone induction by porous glass ceramic made from Bioglass<sup>®</sup> (45S5). *J Biomed Mater Res (Appl Biomater)*. 2001;58:270-6.
- [6] Chen Q, Thompson ID, Boccaccini AR. 45S5 Bioglass<sup>®</sup>-derived glass-ceramic scaffolds for bone tissue engineering. *Biomaterials*. 2006;27:2414-25.
- [7] Vitale-Brovarone C, Verné E, Robiglio L, Appendino P, Bassi F, Martinasso G, Canuto RA. Development of glass-ceramic scaffolds for bone tissue engineering: characterisation proliferation of human osteobasts and nodule formation. *Acta Biomater*. 2007;3:199-208.
- [8] Bellucci D, Chiellini F, Ciardelli G, Gazzarri M, Gentile P, Sola A, Cannillo V. Processing and characterization of innovative scaffold for bone tissue engineering. *J Mater Sci: Mater Med*. 2012;23:1397-409.
- [9] Bairo F, Ferraris M, Bretcanu O, Verné E, Vitale-Brovarone C. Optimization of composition, structure and mechanical strength of bioactive 3-D glass-ceramic scaffolds for bone substitution. *J Biomater Appl*. 2013;27:872-90.
- [10] Gerhardt LC, Boccaccini AR. Bioactive glass and glass-ceramic scaffolds for bone tissue engineering. *Materials*. 2010;3:3867-910.

- [11] Baino F, Vitale-Brovarone C. Three-dimensional glass-derived scaffolds for bone tissue engineering: current trends and forecasts for the future. *J Biomed Mater Res A*. 2011;97:514-35.
- [12] Rahaman MN, Day DE, Bal BS, Fu Q, Jung SB, Bonewald LF, Tomsia AP Bioactive glass in tissue engineering. *Acta Biomater*. 2011;7:2355-73.
- [13] Vitale-Brovarone C, Baino F, Tallia F, Gervasio C, Verné E. Bioactive glass-derived trabecular coating: a smart solution for enhancing osteointegration of prosthetic elements. *J Mater Sci: Mater Med*. 2012;23:2369-80.
- [14] Chen Q, Baino F, Pugno NM, Vitale-Brovarone C. Bonding strength of glass-ceramic trabecular-like coatings to ceramic substrates for prosthetic applications. *Mater Sci Eng C*. 2013;33:1530-8.
- [15] Baino F, Vitale-Brovarone C. Mechanical properties and reliability of glass-ceramic foam scaffolds for bone repair. *Mater Lett*. 2014;118:27-30.
- [16] Wu C, Zhang Y, Zhu Y, Friis T, Xiao Y. Structure-property relationships of silk-modified mesoporous bioglass scaffolds. *Biomaterials*. 2010;31:3429-38.
- [17] Wu C, Fan W, Zhu Y, Gelinsky M, Chang J, Cuniberti G, Albrecht V, Friis T, Xiao Y Multifunctional magnetic mesoporous bioactive glass scaffolds with a hierarchical pore structure. *Acta Biomater*. 2011;7:3563-72.
- [18] Boccaccini AR, Keim S, Ma R, Li Y, Zhitomirsky I. Electrophoretic deposition of biomaterials. *J R Soc Interface*. 2010;7:S581-S613.
- [19] Ducheyne P, Van Raemdonck W, Heughebaert JC, Heughebaert M. Structural analysis of hydroxyapatite coatings on titanium. *Biomaterials*. 1986;7:97-103.
- [20] Zhitomirsky I, Gal-Or L. Electrophoretic deposition of hydroxyapatite. *J Mater Sci: Mater Med*. 1997;8:213-9.

- [21] Krause D, Thomas B, Leinenbach C, Eifler D, Minay EJ, Boccaccini, AR. The electrophoretic deposition of Bioglass particles on stainless steel and Nitinol substrates. *Surf Coating Technol.* 2006;200:4835-45.
- [22] Roether JA, Boccaccini AR, Hench LL, Maquet V, Gautier S, Jerome R. Development and in vitro characterisation of novel bioresorbable and bioactive composite materials based on polylactide foams and Bioglass for tissue engineering applications. *Biomaterials.* 2002;18:3871-8.
- [23] Boccaccini AR, Peters C, Roether JA, Eifler D, Misra SK, Minay EJ. Electrophoretic deposition of polyetheretherketone (PEEK) and PEEK/Bioglass coatings on NiTi shape memory alloy wires. *J Mater Sci.* 2006;41:8152-9.
- [24] Patel KD, El-Fiqi A, Lee HY, Singh RK, Kim DA, Lee HH, Kim HW. Chitosan-nanobioactive glass electrophoretic coating with bone regenerative and drug delivering potential. *J Mater Chem.* 2012;22:24945-56.
- [25] Meng D, Narayan Rath S, Mordan N, Salih V, Kneser U, Boccaccini AR. In vitro evaluation of 45S5 Bioglass<sup>®</sup>-derived glass-ceramic scaffolds coated with carbon nanotubes. *J Biomed Mater Res A.* 2011;99:435-44.
- [26] Vitale-Brovarone C, Baino F, Verné E. High strength bioactive glass-ceramic scaffolds for bone regeneration. *J Mater Sci: Mater Med.* 2009;20:643-53.
- [27] Ma H, Baino F, Fiorilli S, Vitale-Brovarone C, Onida B. Al-MCM-41 inside a glass-ceramic scaffold: a meso-macroporous system for acid catalysis. *J Eur Ceram Soc.* 2013;33:1535-43.
- [28] Baino F, Fiorilli S, Mortera R, Onida O, Saino E, Visai L, Verné E, Vitale-Brovarone C. Mesoporous bioactive glass as a multifunctional system for bone regeneration and controlled drug release. *J Appl Biomater Funct Mater.* 2012;10:12-21.
- [29] Besra L, Liu M. A review on fundamentals and applications of electrophoretic deposition (EPD). *Prog Mater Sci.* 2007;52:1-61.

- [30] Boccaccini AR, Chicatun F, Cho J, Bretcanu O, Roether JA, Novak S, Chen Q. *Adv Funct Mater.* 2007;17:2815-22.
- [31] Thommes M, Kohn R., Froba M. Sorption and pore condensation behavior of pure fluids in mesoporous MCM-48 silica, MCM-41 silica, SBA-15 silica and controlled-pore glass at temperatures above and below the bulk triple point. *Appl Surf Sci.* 2002;196:239–49.
- [32] Kokubo T, Takadama H. How useful is SBF in predicting in vivo bone bioactivity? *Biomaterials.* 2006; 27:2907-15.
- [33] Kenesei P, Kadar C, Rajkovits Z and Lendvai J. The influence of cell-size distribution on the plastic deformation in metal foams. *Scripta Mater.* 2004;50:295-300.
- [34] Karageorgiou V, Kaplan D. Porosity of 3D biomaterial scaffolds and osteogenesis. *Biomaterials.* 2005;26:5474-91.
- [35] Kokubo T, Kushitani H, Ohtsuki C, Sakka S, Yamamuro T. Effects of ions dissolved from bioactive glass-ceramics on surface apatite formation. *J Mater Sci: Mater Med.* 1993;4:1-4.
- [36] Dorozhkin SV. Calcium orthophosphates in nature, biology and medicine. *Materials.* 2009;2:399-498.
- [37] Anselme K, Davidson P, Popa A, Giazson M, Liley M, Ploux L. The interaction of cells and bacteria with surfaces structured at the nanometer scale. *Acta Biomater.* 2010;6:3824-46
- [38] Hench LL, Wilson J. *An introduction to bioceramics.* Singapore: World Scientific; 1993.
- [39] Sepulveda P, Jones JR, Hench LL. In vitro dissolution of melt-derived 45S5 and sol-gel derived 58S bioactive glasses. *J Biomed Mater Res Part A.* 2002; 61: 301-11.
- [40] Pereira MM, Jones JR, Hench LL. Bioactive glass and hybrid scaffolds prepared by sol-gel method for bone tissue engineering. *Adv Appl Ceram.* 2005; 104: 35-42.
- [41] Lopez-Noriega A, Arcos D, Izquiendo-Barba I, Sakamoto Y, Terasaki O, Vallet-Regi M. Ordered mesoporus bioactive glasses for bone tissue regeneration. *Chem Mater.* 2006; 18: 3137-44.

- [42] Pishbin F, Mouriño V, Gilchrist JB, McComb DW, Kreppel S, Salih V, Ryan MP, Boccaccini AR. Single-step electrochemical deposition of antimicrobial orthopaedic coatings based on a bioactive glass/chitosan/nano-silver composite system. *Acta Biomater.* 2013;9:7669-79.
- [43] Verné E, Miola M, Vitale-Brovarone C, Cannas M, Gatti S, Fucale G, Maina G, Massé A, Di Nunzio S. Surface silver-doping of biocompatible glass to induce antibacterial properties. Part I: massive glass. *J Mater Sci Mater Med.* 2009;20:733-40.
- [44] Vitale-Brovarone C, Ciapetti G, Leonardi E, Baldini N, Bretcanu O, Verné E, Baino F. Resorbable glass-ceramic phosphate-based scaffolds for bone tissue engineering: synthesis, properties and in vitro effects on human marrow stromal cells. *J Biomater Appl.* 2011;26:465-89.
- [45] Bretcanu O, Baino F, Verné E, Vitale-Brovarone C. Novel resorbable glass-ceramic scaffolds for hard tissue engineering: from the parent phosphate glass to its bone-like macroporous derivatives. *J Biomater Appl.* 2014;28:1287-303.

## Figure captions

**Figure 1:** SCNA scaffold as such: (a) SEM micrograph of the macroporous architecture (150x); (b) detail of the trabeculae characterized by a surface micro-roughness due to the presence of wollastonite ( $\text{CaSiO}_3$ ) crystals (1200x); (c) EDS analysis carried out on a wollastonite crystal, confirming the predominant presence of Si and Ca (the presence of low peaks of Na and Al, contained in the residual amorphous phase, is due to boundary effects; the peak of Ag is due to the ultrathin metal layer deposited for SEM/EDS analysis).

**Figure 2:** (a) SCNA scaffold coated with MBG by EPD at lower (670x) and (b) higher magnification (4000x); (c) EDS analysis carried out on MBG layer (the presence of low peaks of Na and Al is due to boundary effects of the SCNA substrate).

**Figure 3:** (a) SCNA scaffold coated with MBG by dipping method at lower (400 x) and (b) higher magnification (1500x); (c) EDS analysis carried out on MBG aggregates.

**Figure 4:** Incorporation of MBG inside SCNA scaffolds by “forced” *in situ* gelation: SEM micrographs showing (a) part of the scaffold (44x) and (b) a surface detail before calcination (the SCNA scaffold is completely enveloped by the gel, on which some cracks can be observed); (c) sample surface after calcination (60x) and (d) compositional analysis (EDS) on the MBG fragmented calcined coating (the peak of Ag is due to the ultrathin metal layer deposited for SEM/EDS analysis).

**Figure 5:** Density mapping of MBG-coated SCNA scaffold by micro-CT: (a) 3-D reconstruction of the central (approximately mid-length) cross-sections along the [xy], [xz] and [yz] orthogonal planes and (b) corresponding 2-D development; 3-D reconstruction of three cross-sections along the [xy], [xz] and [yz] orthogonal planes and (b) corresponding 2-D development obtained by placing the analysis plane perpendicular to the EPD flow in a position close to the scaffold outer surface. Different colours (blue and green) are associated to materials with different absorption capacity towards the incident X-rays. Sample dimensions: major size ~8 mm; minor sizes ~4 mm.

**Figure 6:** SEM micrographs of as-such SCNA scaffold after soaking in SBF for (a) 7 days and (b) 1 month (5000X).

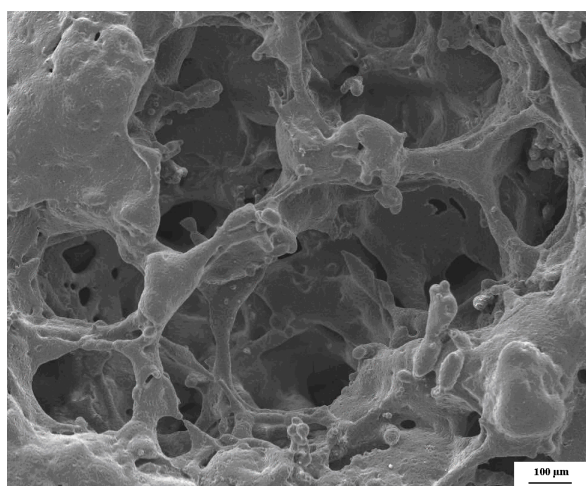
**Figure 7:** SEM micrographs of MBG coated SCNA scaffold after soaking in SBF for 48 h (a) at lower (10000x) and (b) higher magnification (150000x); (c) EDS analysis.

## Tables

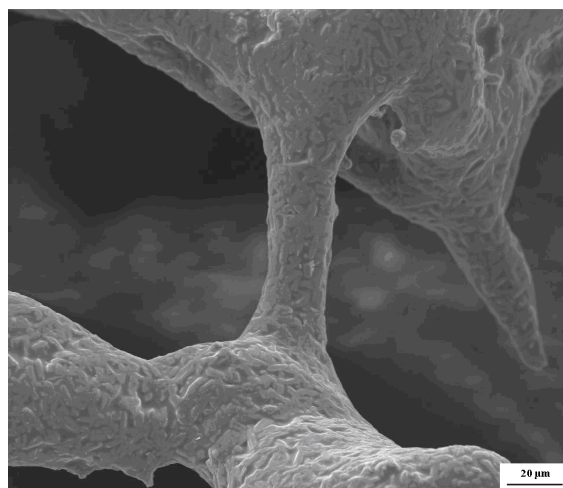
Table 1. Mechanical properties of the prepared scaffolds.

Sample	$\sigma_c$ (MPa)	$E_v (\times 10^6 \text{ J m}^{-3})$
SCNA scaffold as-such	$18.4 \pm 3.7$	$1.5 \pm 0.7$
MBG-coated SCNA scaffold	$19.7 \pm 5.5$	$1.2 \pm 0.7$

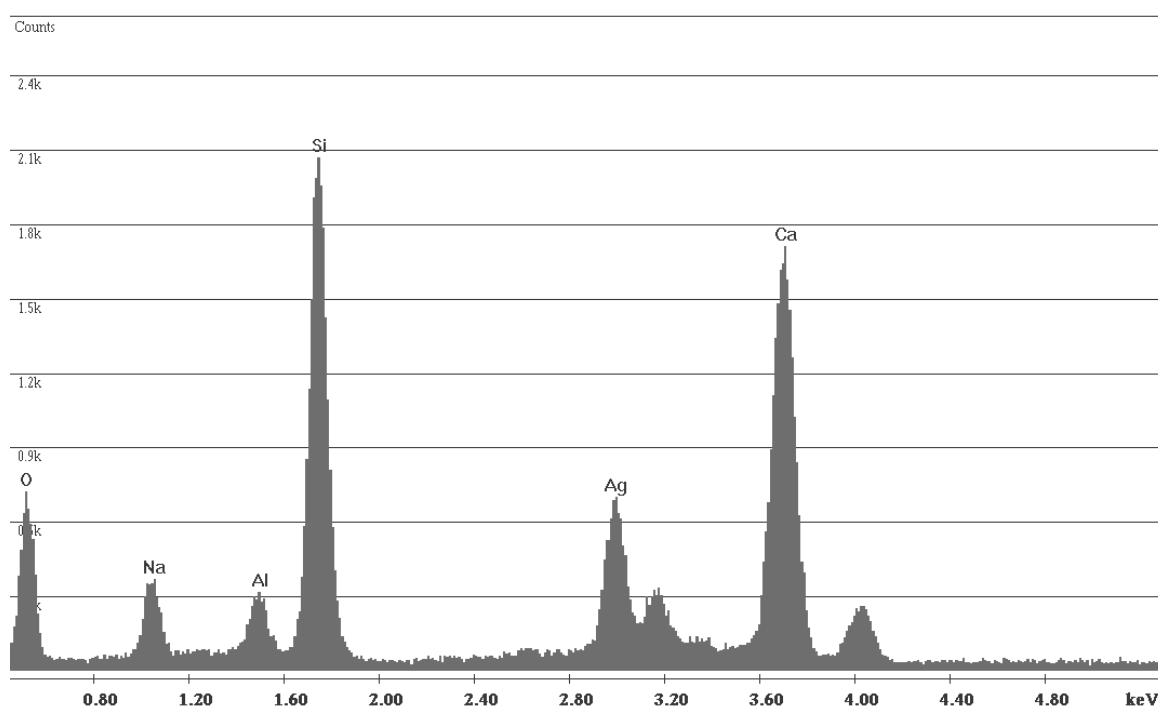
Figure1



(a)



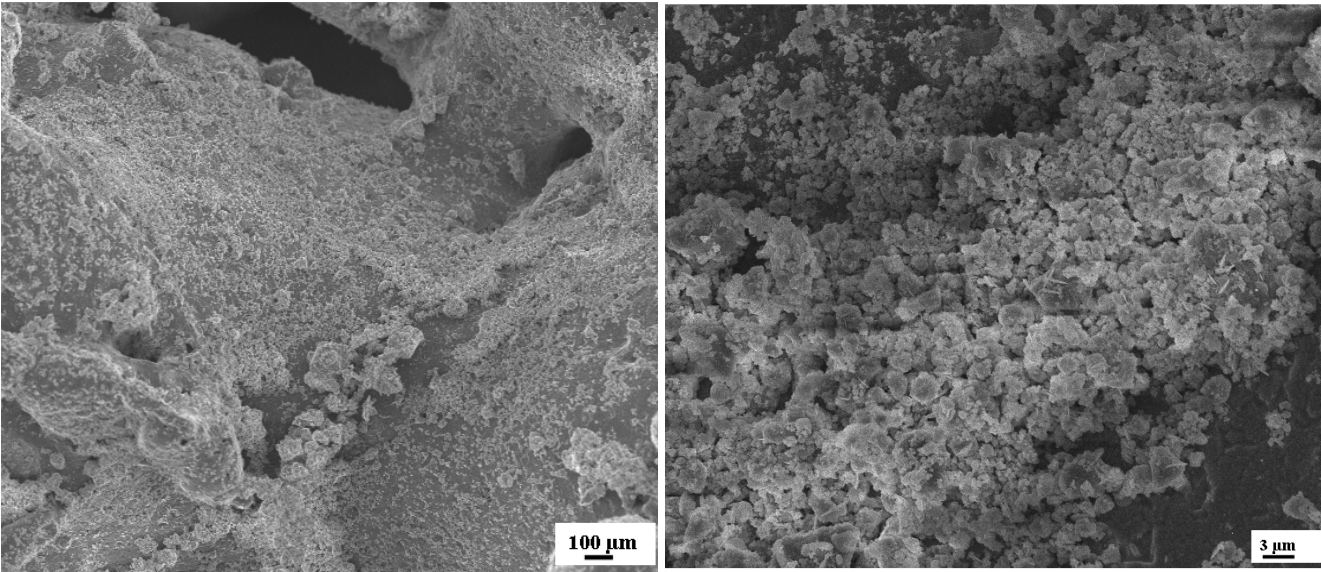
(b)



(c)

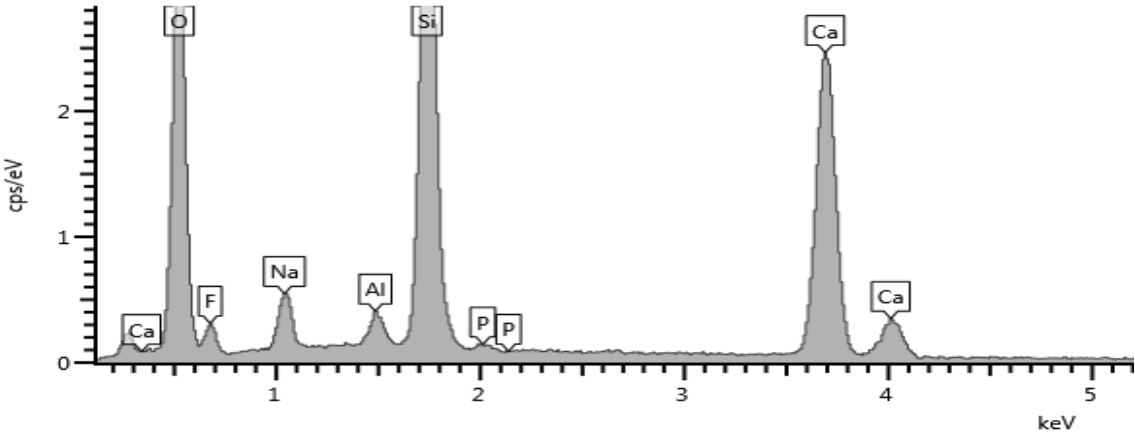


Figure 2



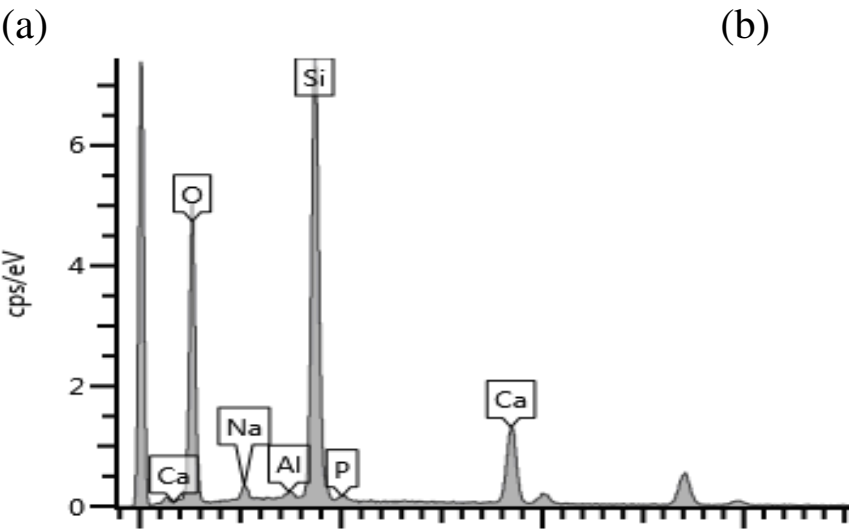
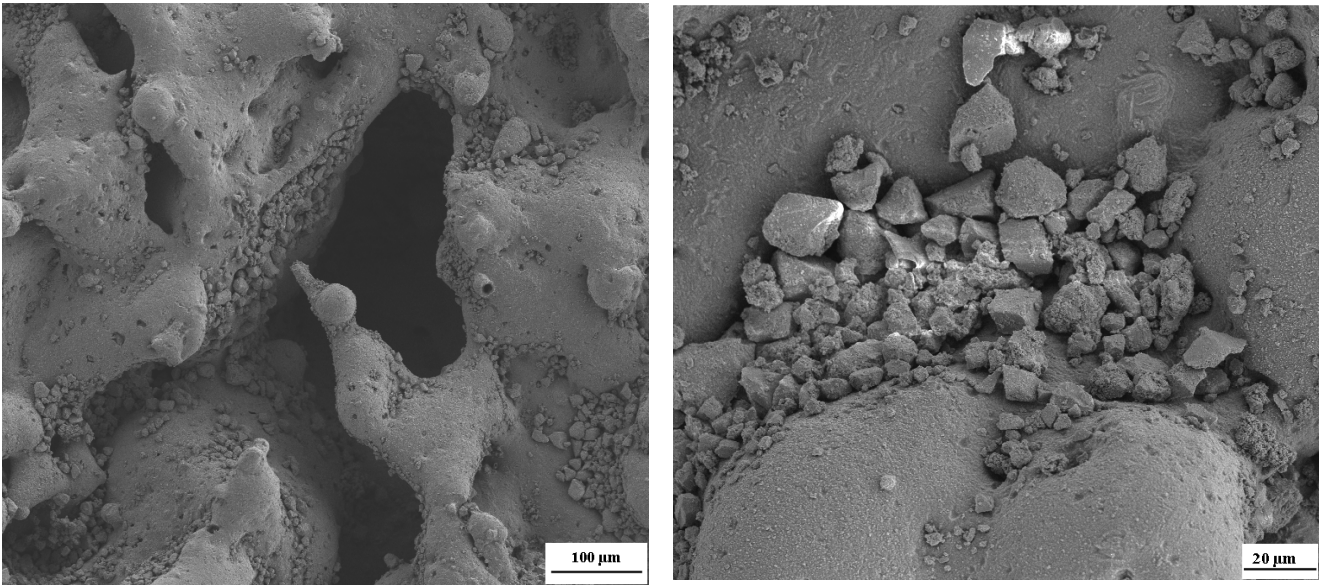
(a)

(b)



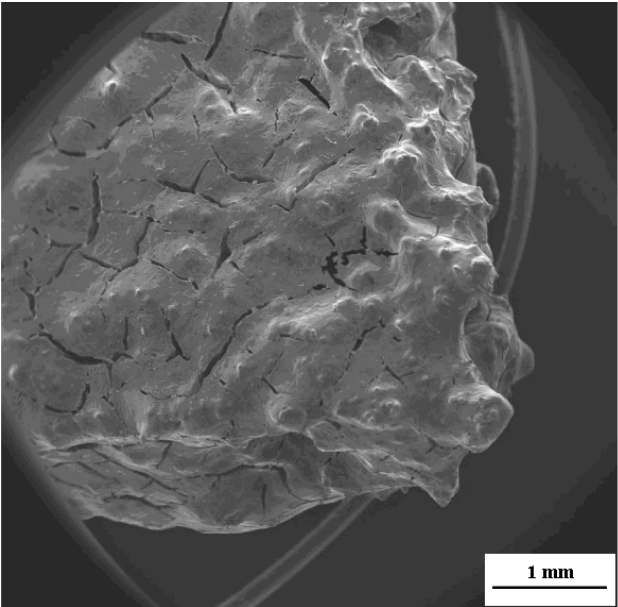
(c)

Figure 3

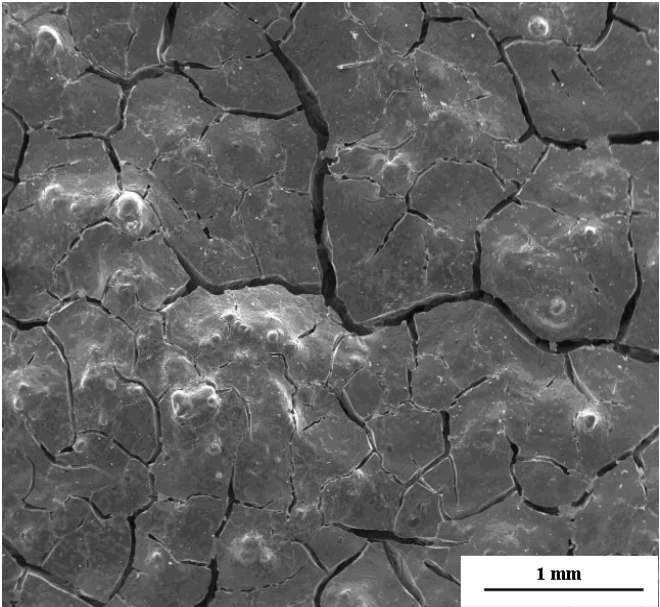


(c)

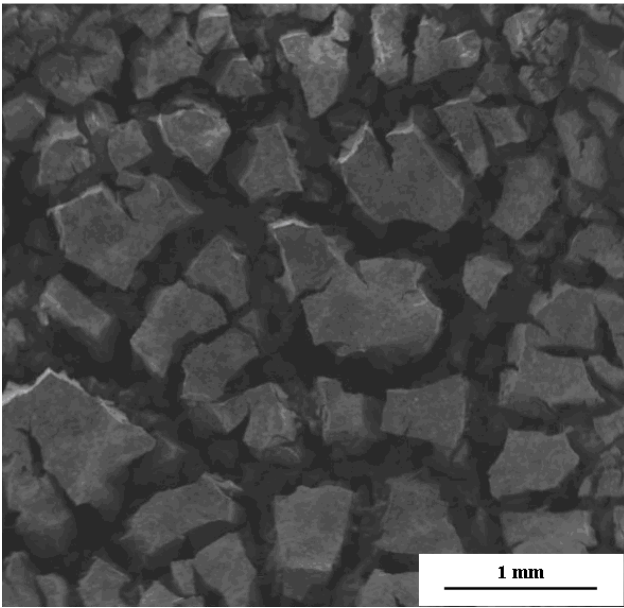
Figure 4



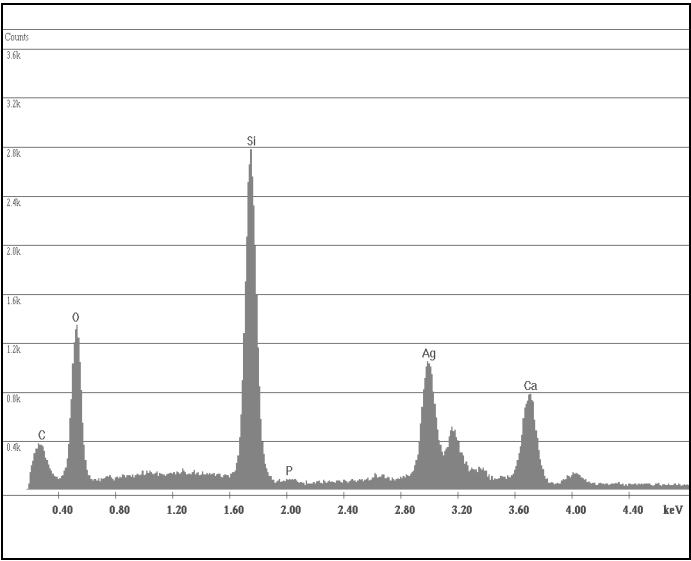
(a)



(b)



(c)



(d)



Figure 5

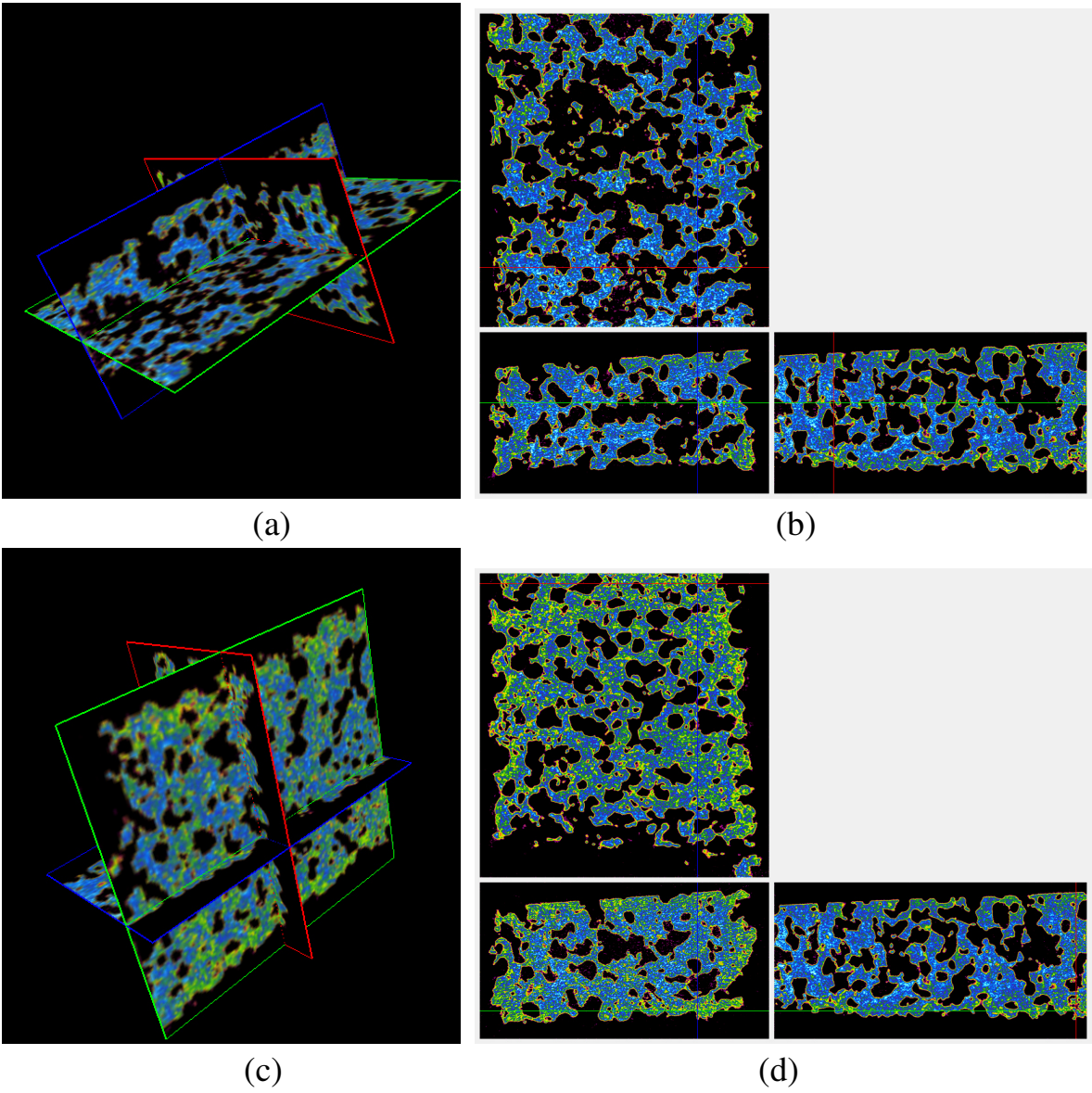
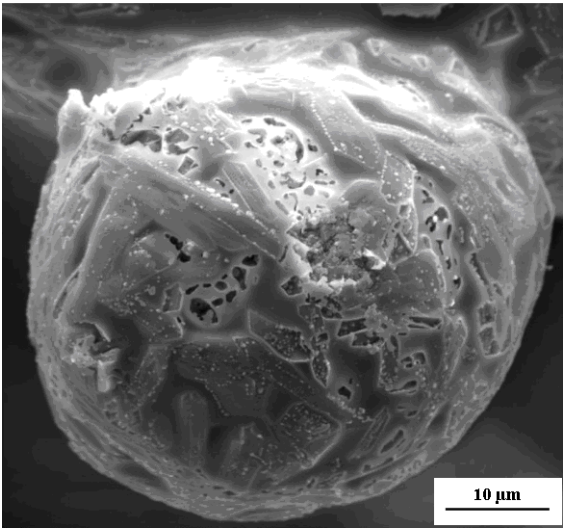
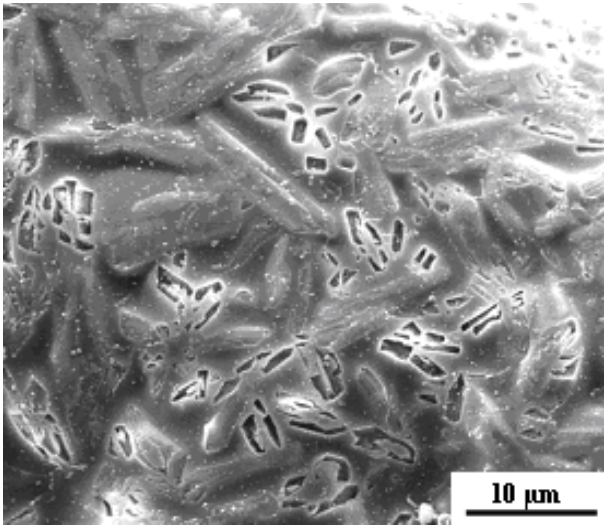


Figure 6

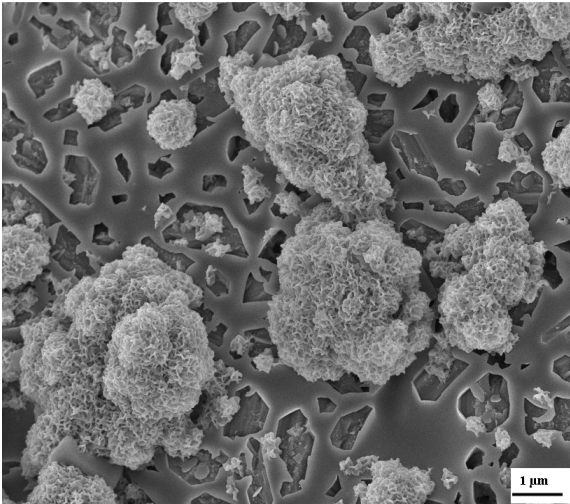


(a)

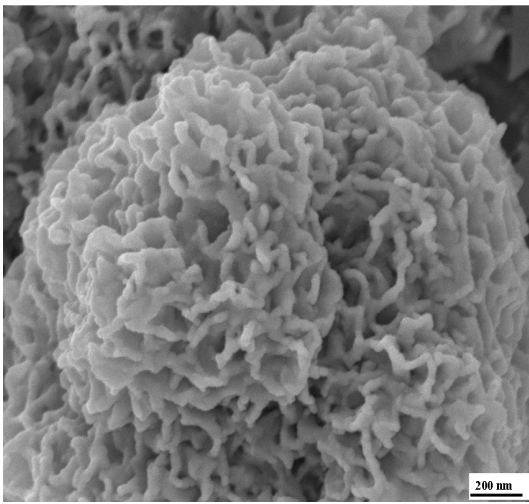


(b)

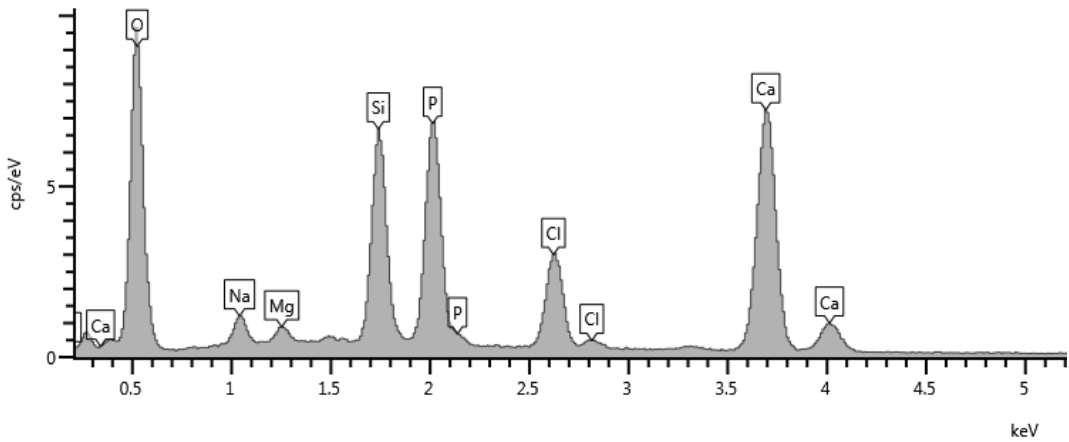
Figure 7



(a)



(b)



(c)